

<https://doi.org/10.1038/s43247-025-02039-0>

Paleoclimate proxy records suggest reduced tropical Pacific zonal asymmetry under sustained global warming

Eui-Seok Chung ^{1,2}, Seong-Joong Kim ^{2,3}✉, Keith B. Rodgers ⁴, Sang-Yoon Jun¹, Joo-Hong Kim¹, Sun-Seon Lee ^{5,6} & Kyung-Sook Yun ^{5,6}

Pronounced model-observation discrepancies in the changes of tropical Pacific zonal sea surface temperature gradient during the satellite era imply systematic model deficiencies. However, the relatively short high-quality instrumental record hampers robustly determining the response of tropical Pacific sea surface temperature to greenhouse gas increases. By adopting paleoclimate proxy records along with a series of climate model simulations, here we show that the zonal gradient is likely to decrease under sustained strong forcing. Paleoclimate proxy records indicate an overall increase of the zonal gradient over time, which has been accompanied by global-mean cooling associated with decreasing carbon dioxide concentrations. Model simulations are found to broadly reproduce the distinct contrast between warmer high carbon dioxide climates and the opposite climates, albeit with large inter-model discrepancy. The qualitative agreement among paleoclimate proxy records and modeled representations therefore lends some important credence to the sign of model-projected future tropical Pacific mean state change.

One of the salient characteristics of the tropical Pacific is a large sea surface temperature (SST) difference between warm waters in the western Pacific warm pool and cold waters in the central-to-eastern tropical Pacific^{1,2}. This zonal SST gradient in the mean state is further enhanced during La Niña events, whereas it weakens substantially during El Niño events. Considering that the tropics can significantly affect extratropical weather and climate via atmospheric teleconnections^{3–6} and that the characteristics of El Niño–Southern Oscillation (ENSO), which is the major predictability source^{1,2}, are closely connected to the tropical Pacific mean state^{1,2,7}, the tropical Pacific SST response to sustained anthropogenic emissions is a component of the climate response that is of particular importance^{8–15}. Under sustained anthropogenic warming, a majority of earlier and current generations of climate models tend to produce a weakened zonal SST gradient across the tropical Pacific^{8,16–20}, which is linked to a weakening of the tropical atmospheric circulation resulting from increased dry static stability²¹ and/or differential atmospheric moisture and precipitation responses²². In contrast, the observational record over the satellite era indicates a distinct strengthening characterized by enhanced warming in the northwest/southwest Pacific but modest cooling in the tropical central-to-eastern Pacific^{6,10–12}, which is accompanied by intensified Hadley and Pacific Walker

circulations^{12,23–25}. Given the close connection between SST and deep convection in the tropics, this model-observation discrepancy has led to a questioning of the credibility of model-projected future climate change^{12,13,17,18,20}.

The enhanced zonal SST gradient that has developed over the satellite era may have resulted from greenhouse gas forcing via ocean memory, with this manifested through either the upwelling of cold subsurface waters along the equatorial Pacific (i.e., an ocean dynamical thermostat mechanism)^{17,26}, a weakening of the amplitude of non-linear ENSO fluctuations²⁷, a strengthened atmospheric circulation¹², a greater warming over the Atlantic and/or Indian Ocean²³, or an enhanced Southern Ocean cooling^{10,11,28}. Such processes may not be accurately represented in climate models, with this resulting in model-observation discrepancies^{17,18,20,29}. Hence, it is possible that there will be La Niña-like SST gradient changes in the future^{8,17}. However, it cannot be ruled out that the enhanced zonal SST gradient has arisen, at least in part, from a transient delay in eastern Pacific warming¹⁹, non-greenhouse gas forcing such as Antarctic stratospheric ozone depletion^{14,30} and anthropogenic aerosols^{19,30–32}, or internal variability^{30,33,34}. These aspects imply that multi-decadal timescales such as the time interval that spans the satellite era might not be long enough to confidently

¹Division of Ocean and Atmosphere Sciences, Korea Polar Research Institute, Incheon, Korea. ²KOPRI School, University of Science and Technology, Incheon, Korea. ³Office of Vice President, Korea Polar Research Institute, Incheon, Korea. ⁴WPI-Advanced Institute for Marine Ecosystem Change, Tohoku University, Sendai, Japan. ⁵Center for Climate Physics, Institute for Basic Science, Busan, Korea. ⁶Pusan National University, Busan, Korea.

✉ e-mail: seongjkim@kopri.re.kr

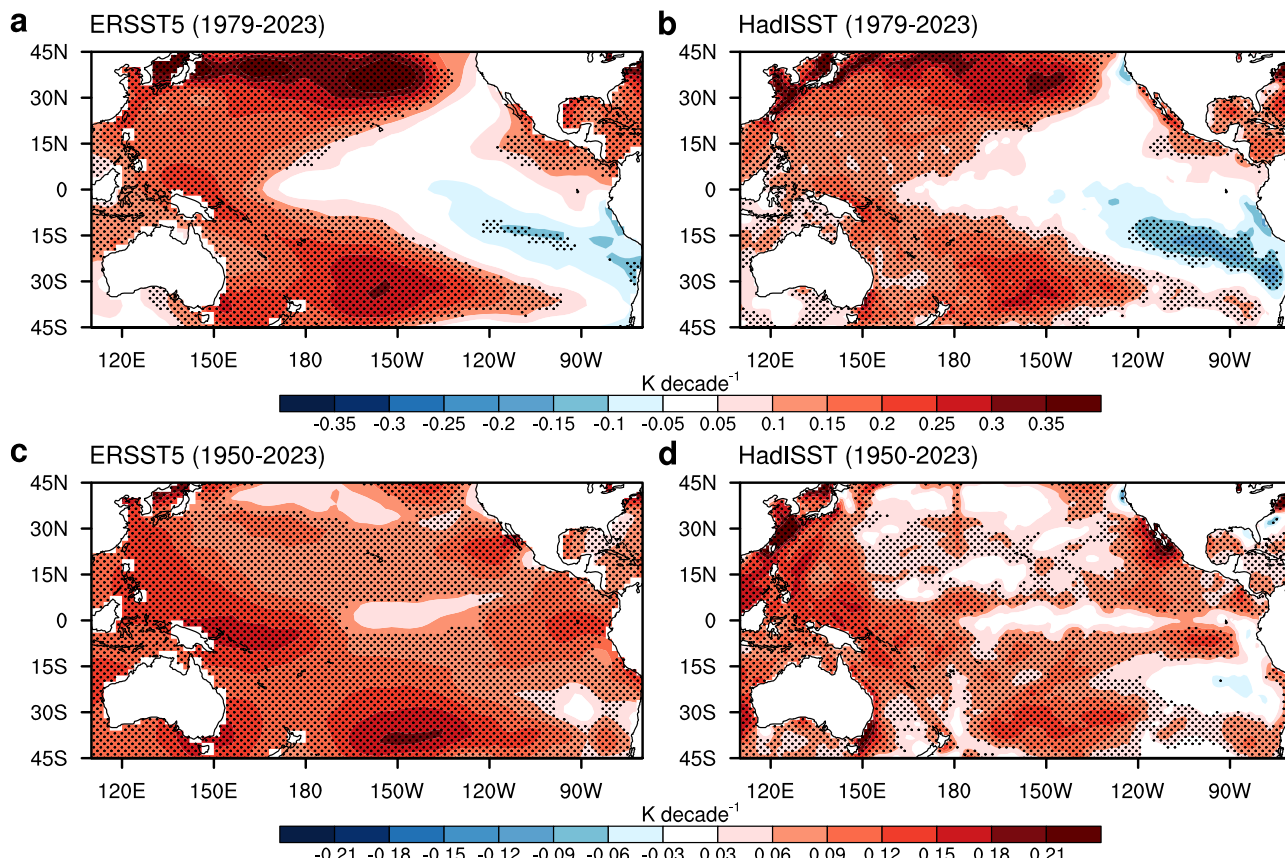


Fig. 1 | Uncertainty in the attribution of observed SST trends over the tropical Pacific. **a** Annual-mean SST trends (units: K decade^{-1}) over the period 1979–2023 computed from ERSST5 with stippling indicating statistical significance of the

computed trends at the 95% confidence level. **b** Same as in **a** but for HadISST. **c** Same as in **a** but over the period 1950–2023. **d** Same as in **b** but over the period 1950–2023.

determine the forced response of the tropical Pacific SST to greenhouse gas forcing. This issue may be resolved by computing centennial trends from reconstructed SST data sets. Potential uncertainties in these data sets, stemming from sparse in-situ measurements in both time and space, especially prior to the 1950s, as well as changes in measurement practice and instrumentation over time, however, hinder unambiguous determination^{35–38}. While some data sets were found to exhibit a reduced zonal SST gradient consistent with a weakening of the Pacific Walker circulation inferred from independent observations of sea level pressure (SLP)³⁹ and surface winds⁴⁰, others exhibit a distinct cooling in the central-to-eastern equatorial Pacific.

In order to take into account the limitations presented by the finite duration of the time of extensive data availability and potential model deficiencies in assessing the zonal SST gradient change resulting from greenhouse gas forcing, we utilized SST reconstructions from paleoclimate proxy records over the past four million years. The utility of the SST reconstruction stems from the large atmospheric carbon dioxide (CO_2) range over the late Cenozoic period, with the magnitude of CO_2 changes comparable to that of projected future changes^{41–43}, and they can thereby provide a unique opportunity for evaluating changes in the zonal SST gradient and thereby help to constrain model performance^{41,42}. In particular, the mid-Pliocene is the most relevant distant past period because atmospheric CO_2 concentrations of ~400 ppm were much higher than under pre-industrial condition^{41,44}. Paleoclimate proxy data over the historical period, rather than over the distant past, might be employed to determine the forced response of the tropical Pacific SST to sustained global warming. However, unambiguous attribution to greenhouse gas forcing may not be feasible due to influences of human-induced non-greenhouse gas forcing agents^{4,19,30–32} and low-frequency internal climate variability^{30,33,34} over the post-war period.

In this study, we first examine whether the time duration of either the satellite or post-war era, over which high-quality SST observations exist, is long enough to unambiguously determine the forced response of tropical Pacific SST to greenhouse gas forcing. Then, we analyze paleoclimate SST records during the mid-Pliocene relative to pre-industrial and assess whether model-simulated changes in the zonal SST gradient under sustained global warming (also under sustained global cooling in the opposite sense) are in line with the change inferred from paleoclimate proxy records. Finally, we explore the temporal evolution of the zonal SST gradient and corresponding global-mean surface temperature over the past four million years in conjunction with a variety of model simulations to determine the sign of the forced response of the zonal SST gradient to large greenhouse gas forcing.

Results

Limitation of instrumental record

We begin by examining observed SST trends over the tropical Pacific. The ERSST5 and HadISST datasets (Methods) indicate a slight cooling in the central-to-eastern tropical Pacific over 1979–2023, which is in stark contrast to pronounced warming in the northwest and southwest Pacific and the western Pacific warm pool (Fig. 1a,b). If this La Niña-like SST trend pattern is a forced signal resulting from anthropogenic global warming, a similar but more pronounced spatial pattern may be expected to have emerged over an extended historical period, such as spanning back to the mid-20th century. However, the spatial pattern over 1950–2023 is noticeably different from that over 1979–2023 and moreover there are disagreements between the reconstructed datasets (Fig. 1c,d). Unlike ERSST5, the HadISST dataset does exhibit an enhanced zonal SST gradient across the equatorial Pacific, and this could reflect an ocean dynamical thermostat mechanism^{17,26}. However, the related muted warming or modest cooling in the central-to-eastern

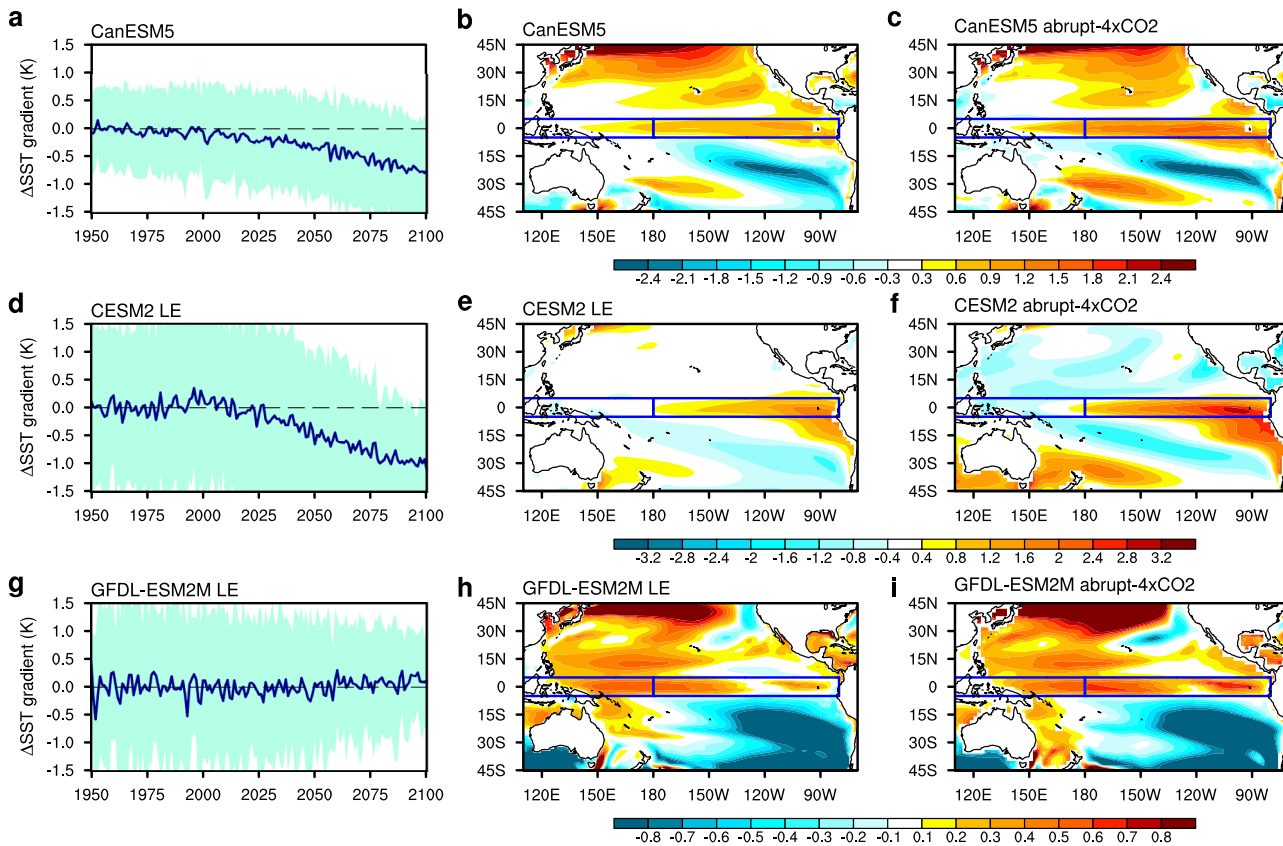


Fig. 2 | Inter-model discrepancies in the forced response of the zonal SST gradient across the equatorial Pacific to greenhouse gas forcing. **a** Changes in the SST difference (units: °K) between the western Pacific (5°S–5°N, 110°E–180°) and the eastern Pacific (5°S–5°N, 180°–80°W) relative to the climatology over 1950–1969 in CanESM5 under the CMIP6 historical protocol (1950–2014) and the SSP3-7.0 (2015–2100) scenario with the line and shading denoting the ensemble mean and two standard deviations across 50 ensemble members. **b** Ensemble-mean SST anomalies averaged over 2081–2100 relative to the climatology over 1950–1969, in which the tropical mean (30°S–30°N) is removed to highlight spatial inhomogeneity.

c SST anomalies averaged over the years 131–150 of the CMIP6 abrupt-4xCO₂ experiment relative to the corresponding pre-industrial control simulation for a single member of CanESM5, in which the tropical mean is removed. **d–f** Same as in **a–c** but for CESM2 and related large ensemble simulations (50 ensemble members with smoothed biomass burning emissions). **g–i** Same as in **a–c** but for GFDL-ESM2M under the CMIP5 historical protocol (1950–2004) and the RCP8.5 (2005–2100) scenario for 30 ensemble members and the abrupt-4xCO₂ (131–150) scenario for a single member.

equatorial Pacific and tropical southeastern Pacific is not statistically significant. Furthermore, corresponding trends in SLP estimated from reanalysis datasets (Methods) indicate a reduced zonal gradient over the tropical Pacific over the post-war period (Supplementary Fig. 1c,d), implying a greenhouse gas forcing-induced weakening of the Pacific Walker circulation^{39,40}, which is at odds with a distinct strengthening over 1979–2023 (Supplementary Fig. 1a,b). It is also noted that surface zonal winds over the central equatorial Pacific exhibit inconsistent trends between the period 1979–2023 and the post-war period (Supplementary Fig. 1, vectors). A previous study³⁸ also showed that instrumental SST records underestimate the 20th century warming trend in the eastern Pacific cold tongue. This raises the question as to whether the La Niña-like SST trend pattern over the satellite era can be attributed solely to greenhouse gas forcing, independent of low-frequency internal variability and non-greenhouse gas forcing^{14,30–34}.

A potential role for low-frequency internal variability and non-greenhouse gas forcing in the La Niña-like SST trend pattern over the satellite era leads us to explore whether the forced response of the zonal SST gradient to anthropogenic forcing has already emerged in large ensemble model simulations (Methods). We identify the timescales over which the forced signal emerges from the background internal variability by comparing the magnitude of the ensemble-mean anomaly relative to the 1950–1969 climatology with two standard deviations across the ensemble members of a given model, with the zonal SST gradient defined, following ref. 34, as the SST difference between the western equatorial Pacific (5°S–

5°N, 110°E–180°) and the eastern equatorial Pacific (5°S–5°N, 180°–80°W). For the case of CanESM5 under historical forcing (up to year 2014) and subsequently the Shared Socioeconomic Pathway (SSP) 3-7.0 (2015–2100) scenario of the Coupled Model Intercomparison Project phase 6 (CMIP6), the ensemble-mean anomalies exhibit a gradual weakening of the zonal SST gradient over time (Fig. 2a), with the ensemble-mean SST change averaged over 2081–2100 clearly indicating more pronounced warming over the eastern equatorial Pacific than over the western equatorial Pacific (Fig. 2b). However, the magnitude of the ensemble-mean change is mostly smaller than the inter-ensemble spread (Fig. 2a), implying the dominance of internal variability over the forced response over the satellite or post-war periods. Although the CESM2 Large Ensemble (CESM2 LE) also projects a distinct reduction in the zonal SST gradient at the end of the 21st century (Fig. 2e), the temporal evolution of ensemble-mean change noticeably differs from CanESM5. The ensemble-mean zonal SST gradient increases from the 1970s to the early 2010s (Fig. 2d), which was attributed to non-greenhouse gas forcing, especially, Antarctic stratospheric ozone depletion and changes in anthropogenic aerosols³⁰, although a marked reduction of the zonal SST gradient eventually follows.

Given well-known model biases (e.g., excessively cold cold-tongue and double inter-tropical convergence zone biases), the zonal SST gradient may strengthen in response to greenhouse gas forcing in reality through mechanisms such as the ocean dynamical thermostat mechanism, inter-basin teleconnection associated with greater warming over the Atlantic and/or Indian Ocean, and ENSO non-linear rectification¹⁵. Indeed, unlike other

climate models participating in CMIP5, GFDL-ESM2M was found to simulate a La Niña-like mean state change under global warming as a result of ENSO non-linear rectification²⁷. Considering that simulation results from a single ensemble member were used in ref. 27, we analyze further the GFDL-ESM2M Large Ensemble (GFDL-ESM2M LE) under CMIP5 historical forcing (1950–2004) followed by the Representative Concentration Pathway (RCP) 8.5 (2005–2100) scenario to determine the forced response of the zonal SST gradient more robustly. Fig. 2g,h indicate a slight increase in the zonal SST gradient at the end of the 21st century relative to the 1950–1969 climatology along with markedly different temporal evolution in comparison to CanESM5 and the CESM2 LE. However, the temporal evolution of the ensemble-mean change does not appear to align with the pathway of greenhouse gas emissions in the RCP8.5 scenario, with the magnitude of the ensemble-mean change being markedly smaller than the inter-ensemble spread even at the end of the 21st century (Fig. 2g). As this indistinct enhancement in the GFDL-ESM2M LE might result from opposing impacts of non-greenhouse gas forcing, the response of the zonal SST gradient to greenhouse gas forcing is additionally explored by analyzing the spatial pattern of SST anomalies relative to pre-industrial conditions in an idealized experiment for which atmospheric CO₂ concentrations were abruptly quadrupled from pre-industrial conditions and then were held fixed for at least 150 years (i.e., abrupt-4×CO₂ scenario). Unlike in Fig. 2h, the SST anomalies averaged over years 131–151 exhibit a slightly greater warming over the central-to-eastern equatorial Pacific than over the western Pacific (Fig. 2i), which is qualitatively consistent with CanESM5 (Fig. 2c) and CESM2 (Fig. 2f). However, the difference between Fig. 2h and Fig. 2i appears to be indistinct. Given the possibility that the changes shown in Fig. 2i might be still far from the full response to the imposed abrupt quadrupling of CO₂, the temporal evolution of simulated zonal SST gradient change is examined over the full simulation period (300 years for GFDL-ESM2M and 999 years for CESM2). As shown in Supplementary Fig. 2a, the change in the zonal SST gradient is distinctly weaker in GFDL-ESM2M in comparison to CESM2. Nevertheless, GFDL-ESM2M also does not indicate a strengthening of the zonal SST gradient in a near-equilibrium climate, which is at odds with Fig. 2g. Furthermore, the SST anomalies averaged over the period 281–300, shown in Supplementary Fig. 2c, more clearly exhibit an enhanced warming in the eastern equatorial Pacific relative to the western equatorial Pacific, which is qualitatively similar to that for CESM2 over 980–999 (Supplementary Fig. 2b) in comparison to Fig. 2i. This suggests that even a centennial timescale might not be long enough to confidently determine the forced response of the zonal SST gradient to greenhouse gas forcing.

Based on the role of the Pacific Walker circulation in shaping the SST distribution in the tropical Pacific, we also examine for the temporal evolution and spatial pattern of model-simulated SLP changes whether the time duration of the instrumental record is long enough to confidently identify the forced response of the Pacific Walker circulation to greenhouse gas forcing (Supplementary Fig. 3). In CanESM5 and the CESM2 LE, the zonal SLP difference between the eastern equatorial Pacific (5°S–5°N, 160°W–80°W) and the western equatorial Pacific (5°S–5°N, 80°E–160°E)³⁹ is projected to distinctly weaken at the end of the 21st century, despite the discrepancy in the trajectory of ensemble-mean change between the two models along with large inter-ensemble spread. In contrast, the GFDL-ESM2M LE simulates a slight strengthening at the end of the 21st century; however, the spatial pattern at the end of the 21st century is inconsistent with that for the abrupt-4×CO₂ experiment, particularly in the western Pacific warm pool, which exhibits an indistinct change or slight weakening. These results therefore indicate that due to the influence of internal variability and non-greenhouse gas forcing, the time duration of the instrumental record covering the satellite or post-war periods might not be sufficiently long to robustly determine the response to greenhouse gas forcing.

Tropical Pacific zonal SST gradient in distant past climates

Having shown the potential limitation of high-quality SST records over the satellite or post-war era, we now turn our attention to paleoclimate proxy

records during the mid-Pliocene warm period as this distant past period with high atmospheric CO₂ concentrations (~400 ppm) may shed light on future change resulting from large greenhouse gas forcing^{44,45}. The PRISM3 SST reconstruction⁴⁶ (Methods) indicates that annual-mean SSTs over the western Pacific warm pool during the mid-Pliocene epoch (~3.3–3.0 million years ago) were similar in magnitude to modern values, with the SST difference (Pliocene minus modern) of 0.2 °K at ODP (Ocean Drilling Program) 769, 0.0 °K at DSDP (Deep Sea Drilling Project) 586 and 0.0 °K at ODP 806 (circles in Fig. 3a). In comparison, the sites located in the eastern tropical Pacific exhibit strongly positive SST anomalies of 2.5 °K at ODP 852, 3.0 °K at ODP 847, 1.9 °K at ODP 677 and 5.4 °K at ODP 1237 except for DSDP 573 (~0.6 °K) (circles in Fig. 3a). The near-zero SST differences in the western Pacific warm pool, but large positive anomalies in the eastern tropical Pacific, are seemingly at odds with what is seen for the present period (Fig. 1a,b).

According to the TEX₈₆-based analyses of ref. 47 (Methods), the western Pacific warm pool was warmer during the late Miocene-to-Pliocene (~12.0–2.6 million years ago) than in the present day, whereas the tropical Pacific zonal SST gradient was not enhanced during these past high CO₂, warm climate states^{47,48}. More specifically, the TEX₈₆-based SST reconstruction (stars in Fig. 3a) indicates that ODP site 806, located in the western Pacific warm pool, had a warmer SST (~1.4 °K) 3.17 million years ago relative to 0.1 million years ago. A larger SST difference of ~2.9 °K between 3.16 million years ago and 0.14 million years ago was, however, estimated at ODP site 850, located in the eastern equatorial Pacific, suggesting a reduced zonal SST gradient during the mid-Pliocene period.

Given the potential cold bias of TEX₈₆ paleotemperature data, especially over the eastern equatorial Pacific⁴⁵, as well as the uncertainties inherent in Mg/Ca paleotemperature data due to changes in seawater Mg/Ca ratio over time^{45,47}, ref. 44 reconstructed SST records based solely on alkenone ($U_{37}^{K'}$) paleotemperature data using a Bayesian calibration method to account for the upper limit issue of alkenone-based estimation (Methods). Their reconstruction also indicates a reduced zonal SST gradient during the mid-Pliocene period relative to pre-industrial conditions (triangles in Fig. 3a): although ODP site 806 exhibited a warmer SST (~1.1 °K) during the mid-Pliocene warm period around 3.2 million years ago relative to the pre-industrial state, the sites located in the eastern Pacific were estimated to have warmer SST anomalies than the western Pacific site (i.e., ODP 806) except for IODP (Integrated Ocean Drilling Project) site U1338 (ODP 846: ~3.6 °K, ODP 847: ~2.2 °K, ODP 850: ~1.7 °K, ODP 1237: ~1.9 °K, ODP 1239: ~2.4 °K, ODP 1241: ~1.4 °K, IODP U1338: ~0.7 °K). Therefore, despite substantial discrepancies in the magnitude between the studies, paleoclimate proxy records during the mid-Pliocene warm period collectively suggest that the zonal SST gradient is predisposed to weaken during warm climate states with high CO₂ levels relative to colder climates with lower CO₂.

Next, on the premise that there is a causal relationship between CO₂ forcing and changes in the tropical Pacific zonal SST gradient, we qualitatively evaluate the fidelity of model simulations using mid-Pliocene paleoclimate proxy records as a benchmark. Consistent with the PRISM3, TEX₈₆-based and alkenone-based SST reconstructions, the CESM2 model simulates positive SST anomalies over the tropical Pacific under the CMIP6 Paleoclimate Modelling Intercomparison Project phase 4 (PMIP4) midPliocene-eoi400 scenario (Methods) relative to pre-industrial conditions, with more pronounced warming in the central-to-eastern tropical Pacific than in the western Pacific warm pool (shading in Fig. 3a). Although the spatial pattern and magnitude of simulated tropical SSTs exhibit substantial inter-model spread, other models contributing to CMIP6-PMIP4 simulate a reduced zonal SST gradient (or at least enhanced warming in the eastern equatorial Pacific which is at odds with the La Niña-like SST change pattern over the satellite era) during the mid-Pliocene warm period relative to the pre-industrial state (Supplementary Fig. 4).

Despite an overall reduction in the zonal SST gradient in both paleoclimate proxy records and model simulations, paleoclimate proxy records exhibit indistinct warm anomalies over part of the eastern equatorial Pacific

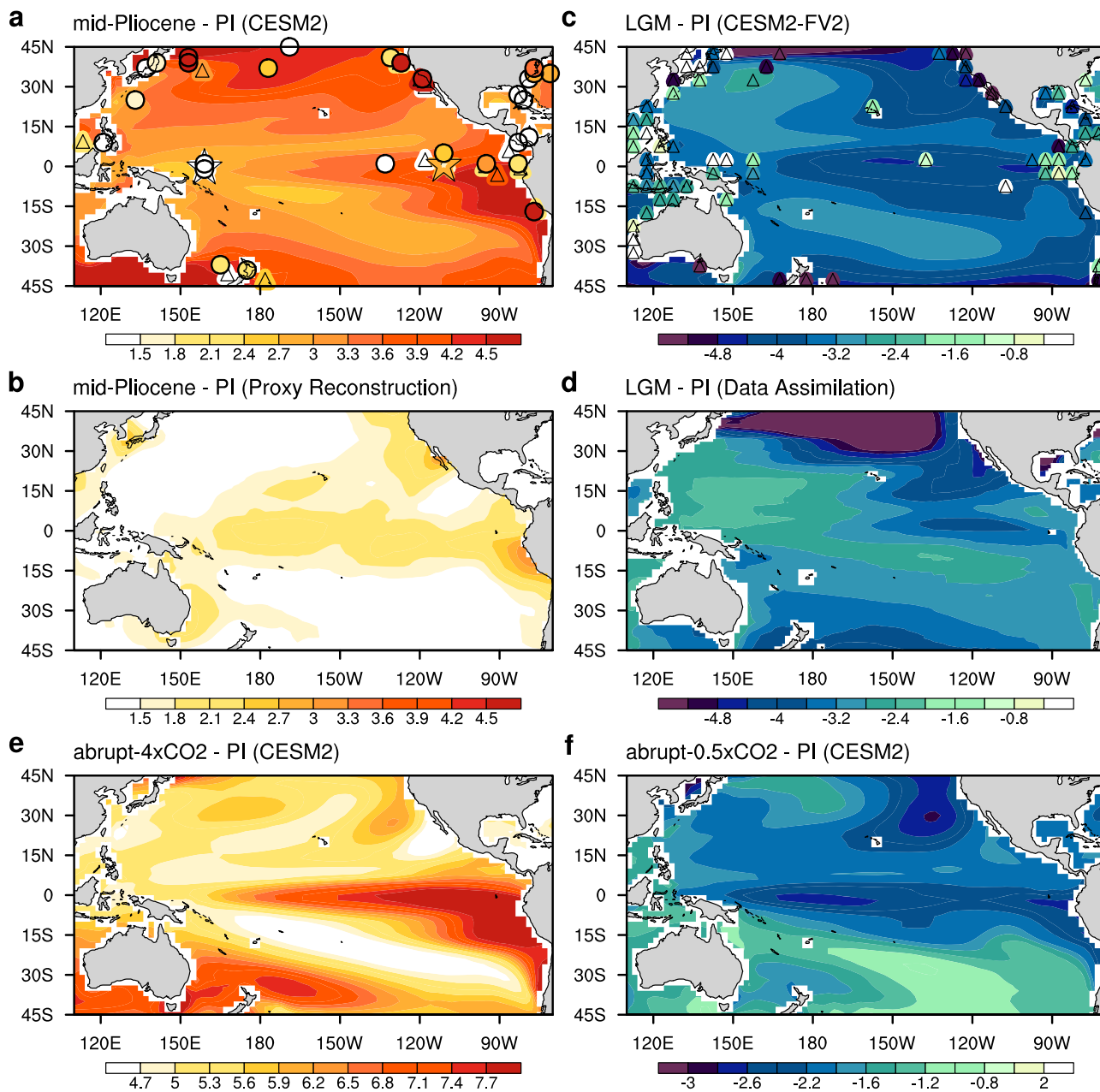


Fig. 3 | Zonal contrast in the annual-mean SST anomalies in the tropical Pacific. **a** Mean SST differences (units: °K) for CESM2 between the CMIP6 mid-Pliocene-*eo1400* and pre-industrial control simulations. Superimposed circles, stars and triangles represent, respectively, the SST anomalies (mid-Pliocene minus modern) from the PRISM3 dataset, the SST anomalies (~3.2 million years ago minus ~0.1 million years ago) from TEX₈₆ (TetraEther indeX of 86 carbons)-based reconstructions⁴⁷, and the SST anomalies (~3.2 million years ago minus pre-industrial) inferred from the alkenone paleotemperature proxy⁴⁴. **b** Reduced space reconstruction of SST differences, derived from alkenone proxy data, between the

mid-Pliocene and pre-industrial conditions (ref. 44). **c** Mean SST differences for CESM2-FV2 between the CMIP6 lgm and pre-industrial control simulations. Superimposed triangles represent the SST anomalies inferred from geochemical proxy data (ref. 49). **d** Similar to c but for the average of three paleoclimate data assimilation products, i.e., ref. 49, ref. 51 and ref. 52. **e** Mean SST differences for CESM2 between the CMIP6 abrupt-4xCO₂ (averaged over the years 131–150) and pre-industrial control simulations. **f** Mean SST differences for CESM2 between the CMIP6 abrupt-0.5xCO₂ (averaged over the years 131–150) and pre-industrial control simulations.

in comparison to model simulations (Fig. 3a). Considering that the accuracy of paleotemperature reconstructions can be affected by a variety of factors, we also analyzed a reconstructed Pliocene Pacific SST field derived from alkenone proxy data⁴⁴. As reported in ref. 44, Fig. 3b more clearly indicates a reduced zonal SST gradient during the mid-Pliocene warm period.

The paleoclimate proxy records during the mid-Pliocene warm period conversely imply an enhanced zonal SST gradient during colder climates with lower CO₂ levels. Considering that the Last Glacial Maximum (LGM) was characterized by a much colder climate with lower CO₂ levels (~200 ppm) relative to pre-industrial conditions, the PMIP community has

selected the LGM as a particularly relevant past period for understanding near-future climate change⁴¹. Hence, we also analyzed CMIP6-PMIP4 lgm simulations along with proxy records to assess the robustness of the conclusion drawn from Fig. 3a,b and Supplementary Fig. 4.

As CMIP6-PMIP4 lgm scenario simulations were not performed with CESM2, we used output from CESM2-FV2 and CESM2-WACCM-FV2, with both of these representing similar climate states to CESM2. For both CESM2-FV2 (Fig. 3c) and CESM2-WACCM-FV2 (Supplementary Fig. 5a), the SST differences between the lgm and pre-industrial experiments exhibit negative values in the tropical Pacific with more enhanced cooling in the

central-to-eastern Pacific than in the western Pacific warm pool, which qualitatively aligns with inferences from the paleoclimate proxy records during the mid-Pliocene warm period. The contrast in the zonal SST gradient change between the mid-Pliocene and LGM periods is qualitatively consistent with the difference between two idealized CO₂-only experiments of CMIP6, one with atmospheric CO₂ concentrations instantaneously quadrupled from pre-industrial levels (i.e., abrupt-4×CO₂; Fig. 3e) and the other where concentrations were instantaneously halved (i.e., abrupt-0.5×CO₂; Fig. 3f). These qualitative similarities appear to indicate that the trajectory of large atmospheric CO₂ changes has played a major role in governing the change in the zonal SST gradient across the equatorial Pacific in the distant past, although climate change during the LGM is of course also linked to other factors including orbital parameters, ice sheet, and land-sea configuration⁴¹. Note that the enhanced cooling in the central-to-eastern equatorial Pacific is also represented by INM-CM4-8 and MIROC-ES2L (Supplementary Fig. 5b,c). In comparison, the spatial distribution of SST anomalies over the tropical Pacific for MPI-ESM1-2-LR differs from other models; however, an enhanced cooling in the eastern equatorial Pacific is also evident (Supplementary Fig. 5d). Moreover, as in other climate models providing simulation output for both abrupt-4×CO₂ and lgm or mid-Pliocene-eoi400, MPI-ESM1-2-LR also exhibits a reduced zonal SST gradient in response to a quadrupling of atmospheric CO₂ concentrations (Supplementary Fig. 6).

In comparison, SST anomalies in the LGM period, inferred from geochemical proxy records⁴⁹, exhibit an indistinct change in the zonal SST gradient, although the zonal SST gradient does not appear to have increased (Fig. 3c, triangles). While there has been a lack of consensus on the spatial distribution of SST anomalies over the tropical Pacific during the LGM due to conflicting proxy reconstructions^{49,50}, such large uncertainties have been substantially reduced by the paleoclimate data assimilation technique. Indeed, the SST anomalies during the LGM averaged over three paleoclimate data assimilation products^{49,51,52} indicate enhanced cooling in the eastern equatorial Pacific relative to the western equatorial Pacific (Fig. 3d), which is supported by an independent study⁵⁰ indicating a deepened mixed layer induced by a stronger Pacific Walker circulation during the LGM in comparison to pre-industrial or current conditions.

Despite a qualitatively similar increase in the zonal SST gradient between Fig. 3c and Fig. 3d, we note that there is a noticeable discrepancy in the spatial pattern: while the paleoclimate data assimilation products suggest the strongest LGM cooling in the eastern equatorial Pacific, CESM2-FV exhibits strong cooling in both the central and eastern equatorial Pacific. Likewise, although the zonal SST gradient is enhanced in both Fig. 3c,d (i.e., LGM) and Fig. 3f (abrupt-0.5×CO₂ experiment), the cooling is weaker at the dateline in comparison to 150°W along the equator in the former but stronger in the latter. These discrepancies might have resulted from model deficiency or suggest that the zonal SST gradient change during the LGM period might not be consistent with that for the halved CO₂-only experiment.

Changes in the zonal SST gradient and global-mean surface temperature over the late Cenozoic

We also consider whether the reduced zonal SST gradient during the mid-Pliocene warm period may have existed independently of warmer global temperatures by analyzing changes in the zonal SST gradient and global-mean surface temperature over the past four million years. A variety of paleoclimate proxy records suggest an overall cooling of global-mean surface temperature over the past four million years (Supplementary Fig. 7a). Despite discrepancies in the magnitude of estimated cooling between studies⁴³, this cooling over time has been linked, in large part, to decreased atmospheric CO₂ concentrations (Supplementary Fig. 7b)⁴³.

According to the alkenone-based SST reconstructions of ref. 44, the SST difference between the western Pacific warm pool and the eastern equatorial Pacific has undergone an overall increase during the late Cenozoic period, albeit with substantial temporal variations (Supplementary Fig. 7c, purple line). Also presented in Supplementary Fig. 7c is a time series

of the zonal SST difference estimated by ref. 43, in which Mg/Ca ratio and faunal proxies were used together with alkenone-based proxies to reconstruct global and regional SSTs. Due to differences in proxies, core sites and calibration methods between ref. 43 and ref. 44, the time series exhibit substantial discrepancies. However, the zonal SST difference based on the reconstruction of ref. 43 also indicates an overall increase over the same period, which is further supported by ref. 45 and ref. 47. Hence, the zonal SST difference appears to have strengthened in response to global cooling. To show this aspect more quantitatively, a scatter plot is created using the reconstruction of ref. 43 over the past four million years. Figure 4a indicates that although there is a large spread, the zonal SST difference tends to have weakened during warm climate states in comparison to much colder climates in the distant past. More specifically, the reconstruction of ref. 43 suggests that the SST difference between the western Pacific warm pool and the equatorial eastern Pacific has decreased by ~0.3 °K with respect to a 1-K increase in global-mean surface temperature (Fig. 4a). The zonal SST differences estimated from the reconstruction of ref. 44 points to a similar conclusion with a nearly identical regression slope, albeit with some non-linearity (Fig. 4b).

Next, we show that climate models are able to broadly reproduce the relationship inferred from paleoclimate proxy records. In Fig. 4c, model-simulated zonal SST gradient is related to corresponding global-mean surface air temperature for midPliocene-eoi400 (filled triangles in red), lgm (filled triangles in blue), abrupt-4×CO₂ (open squares in red), abrupt-0.5×CO₂ (open squares in blue), abrupt-solp4p (similar to abrupt-4×CO₂, except that the solar constant was instantaneously increased by 4%, open circles in red) and abrupt-solm4p (similar to abrupt-4×CO₂, except that the solar constant was instantaneously reduced by 4%, open circles in blue). Although the contrast between midPliocene-eoi400 and lgm is less distinct in comparison to both abrupt-4×CO₂/abrupt-0.5×CO₂ and abrupt-solp4p/abrupt-solm4p, model simulations are roughly consistent with paleoclimate proxy records in that the tropical Pacific zonal SST gradient tends to weaken under sustained global warming and vice versa, although the regression slope is just around -0.1 K K^{-1} . The smaller magnitude compared to the paleoclimate proxy records implies that climate models might underestimate the response of the zonal SST gradient to global warming. Fig. 4d indicates that the weakening of the zonal SST gradient under sustained global warming is in general accompanied by a slowdown of the Pacific Walker circulation. Although the contrast in the SLP gradient change between midPliocene-eoi400 and lgm is again less distinct, climate models, for which simulation output for abrupt-4×CO₂ is available, are found to exhibit a distinctly weakened zonal SST gradient in response to CO₂ quadrupling (Supplementary Fig. 6).

Finally, based on the qualitative agreement of CESM2 with mid-Pliocene proxy records (Fig. 3a,b), simulated changes in SLP and 850-hPa winds under midPliocene-eoi400 relative to pre-industrial experiment are compared with ensemble-mean changes for year 2100. Although the simulated changes are not identical, both distant past and future warm periods are characterized by an overall weakening of the Pacific Walker circulation (Supplementary Fig. 8a,b), in line with previous studies^{39,40,44,53}. It is also noted that both distant past and future simulations exhibit an increased freshwater forcing over the central-to-eastern equatorial Pacific in warm climates (Supplementary Fig. 8c,d), which can be expected to impede the upwelling of cold subsurface waters.

Summary and Discussion

Considering the far-reaching influences of the tropical Pacific SSTs, the marked model-observation discrepancy in the changes of the zonal SST gradient across the tropical Pacific over the satellite era could potentially undermine our confidence in model-projected human-induced future climate change. However, we found large inter-model discrepancies in the temporal evolution of the forced response of the zonal SST gradient in large-ensemble model simulations along with substantial inter-ensemble spread. In addition, it is found that GFDL-ESM2M also eventually exhibits a slight weakening of the zonal SST gradient in response to CO₂ quadrupling,

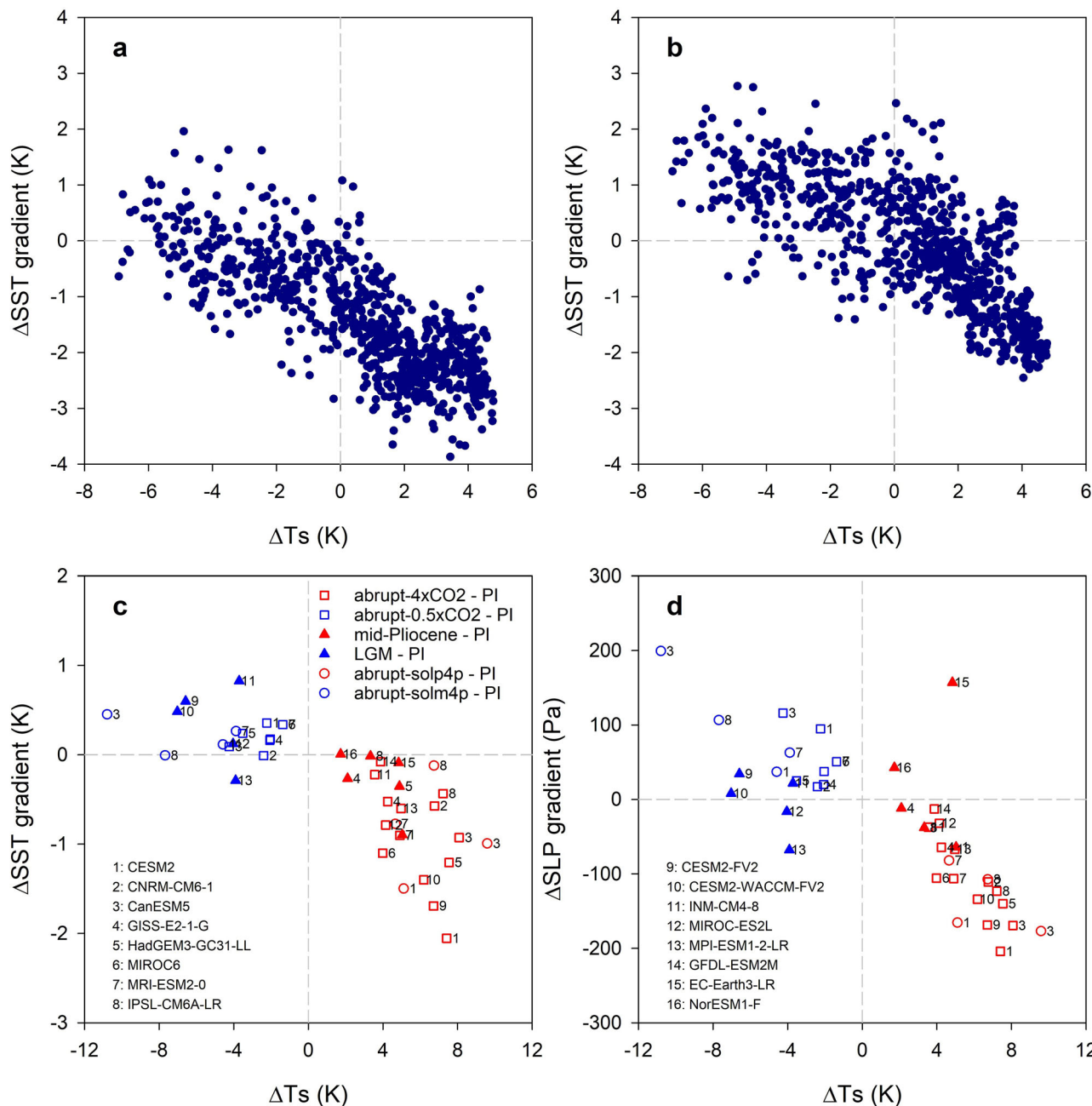


Fig. 4 | Changes in the zonal SST gradient across the equatorial Pacific in response to global warming. **a** A scatter plot highlighting changes in the zonal SST gradient relative to pre-industrial versus corresponding global-mean surface temperature change over the past four million years based on the reconstruction of ref. 43. **b** Same as in **a** but with change in the zonal SST gradient based on the reconstruction of ref. 44. **c** Model-simulated response of the SST difference between the western Pacific (5°S–5°N, 110°E–180°) and the eastern Pacific (5°S–5°N, 180°–80°W) to global warming. Open squares in red (blue) denote the SST anomalies averaged over the years 131–150 of abrupt-4xCO₂ (abrupt-0.5xCO₂) relative to the

corresponding pre-industrial control simulation for a given model. Filled triangles in red (blue) represent the SST differences between the mid-Pliocene-eo400 (lgm) and pre-industrial control simulations. Open circles in red (blue) denote the SST anomalies averaged over the years 131–150 of abrupt-solp4p (abrupt-solm4p) relative to the corresponding pre-industrial control simulation for a given model. Each number in the figure denotes a distinct climate model. **d** Same as in **c** but for the SLP differences between the eastern Pacific (5°S–5°N, 160°W–80°W) and the western Pacific (5°S–5°N, 80°E–160°E).

thereby differing from the slight strengthening at the end of the 21st century for the same model, implying that timescales longer than a century might be needed to confidently identify the forced response to greenhouse gas forcing. The finding of previous studies that the observed La Niña-like SST trend pattern is linked in part to non-greenhouse gas forcing^{14,19,30–32} further complicates this challenge. Due to this potential limitation of the effective duration over which high-quality historical SST observations exist, we analyzed the response of the tropical Pacific SST to large past climate changes using paleoclimate proxy records over the past four million years.

Paleoclimate proxy records indicate that the tropical Pacific zonal SST gradient weakened during high CO₂ warm periods, such as the mid-Pliocene, relative to colder periods with lower CO₂ levels. We found that idealized climate model simulations are able to broadly capture this contrasting feature. Synthesizing all of these results therefore leads us to conclude that the tropical Pacific zonal SST gradient is likely to decrease under sustained large global warming.

Previous studies suggested that both the ocean dynamical thermostat linked to ocean thermal stratification²⁶ and the tropical atmospheric

circulation, especially the Pacific Walker circulation²², govern the response of tropical Pacific SST to external forcing^{16,35}. In other words, the zonal SST gradient can be enhanced in response to greenhouse gas forcing if the ocean dynamical thermostat dominates over a weakened Pacific Walker circulation, and vice versa. The results inferred from paleoclimate proxy data seem to suggest that the ocean dynamical thermostat could play a dominant role at first but its influence might diminish under sustained global warming with continued emissions of greenhouse gases^{16,19,35}. In addition to increased dry static stability²¹ and/or differential atmospheric moisture and precipitation responses²², enhanced warming over the extra-tropics relative to the tropics might lead to a slowdown of the Pacific Walker circulation under sustained global warming, i.e., weakened mid-latitude westerlies due to reduced meridional temperature gradient may induce changes in subtropical anticyclonic circulations and related Pacific trade winds.

Although paleoclimate proxy records during the mid-Pliocene warm period consistently imply a weakening of the zonal SST gradient with global warming, substantial uncertainties remain in terms of the spatial pattern and magnitude due to uneven proxy data sampling in both space and time, proxy uncertainties and methodological limitations^{42,43,45,47}. Thus, as a complement to developments with research efforts in modeling, concurrent continued expansion of the spatio-temporal resolution of paleo-proxy records needed for determining more spatially and temporally coherent climate response to external forcing, as well as the accuracy of these records, will constitute an essential contribution to advancing our understanding of the response of tropical Pacific SST to sustained anthropogenic forcing.

Methods

Observed SST data and paleoclimate SST proxy records

Tropical Pacific SST trends are analyzed using NOAA's Extended Reconstructed Sea Surface Temperature version 5 (ERSST5)⁵⁴, which covers the period from 1854 to present, along with the Hadley Centre Sea Ice and Sea Surface Temperature (HadISST) SST dataset⁵⁵, which covers the period from 1870 to present. For estimating SLP trends, the European Centre for Medium-Range Weather Forecasts Reanalysis version 5 (ERA5) dataset⁵⁶ and the Japanese 55-year Reanalysis (JRA-55)⁵⁷ are used in this study. ERA5 and JRA-55 use HadISST2 and COBE (Centennial in situ Observation-Based Estimates) SST, respectively, for boundary conditions. Hence, there might be a mismatch between SST trends shown in Fig. 1 and SLP trends shown in Supplementary Fig. 1. However, both ERA5 and COBE-SST2⁵⁸ indicate that the La Niña-like SST trend pattern over 1979–2023 is not evident over 1950–2023 (Supplementary Fig. 9).

To explore the SST difference between the western Pacific warm pool and the eastern tropical Pacific during the mid-Pliocene epoch (~3.3–3.0 million years ago), we used the Pliocene Research Interpretation and Synoptic Mapping (PRISM, version 3) annual mean SST data products available through the Deep Sea Drilling Project (DSDP) and Ocean Drilling Program (ODP) sites. These products were estimated from foraminifera, radiolarian, diatom, ostracod, the Mg/Ca ratio of planktic foraminifera, and the unsaturation index of alkenones^{46,59,60}. The PRISM3 sites located in the western Pacific warm pool are ODP 769 (8.78°N, 121.29°E), DSDP 586 (0.50°S, 158.50°E), and ODP 806 (0.31°N, 159.36°E) and the sites located in the eastern tropical Pacific include DSDP 573 (0.49°N, 133.30°W), ODP 852 (5.28°N, 110.07°W), ODP 847 (0.18°N, 95.32°W), ODP 677 (1.20°N, 83.74°W), and ODP 1237 (16.00°S, 76.37°W). With PRISM3^{46,59,60}, the modern SST fields used to remove differences inherent in proxy calibrations are from ref. 61 for SST proxies based on the Mg/Ca ratio of planktic foraminifera and the unsaturation index of alkenones, and from ref. 62 for faunal-based SST proxies.

The accuracy of paleotemperature reconstructions can be affected by diagenetic overprinting, changes in seawater chemistry, and calibration limitations^{42,43,47,49}. Given the possibility that proxy-based SSTs in the western Pacific warm pool might be underestimated for warm climate states in the distant past due to both changes in seawater Mg/Ca ratio and the upper limit of alkenone-based temperatures (~28.5 °C or ~301.65 °K), ref. 47 reconstructed SST for the past 12 million years using both TEX₈₆

(TetraEther indeX of 86 carbons) with the temperature calibration of ref. 63 and alkenone temperature proxies at ODP sites 769, 806, and 1143 (9.36°N, 113.29°E) in the western Pacific warm pool and ODP site 850 (1.30°N, 110.52°W) in the eastern tropical Pacific. This proxy dataset constructed by ref. 47 is also used in our analysis.

Due to potential cold bias of TEX₈₆-based paleotemperature data, especially over the eastern equatorial Pacific⁴⁵, and uncertainties in Mg/Ca paleotemperature data^{45,47}, ref. 44 reconstructed SST records using only alkenone proxies with a Bayesian calibration method to account for the upper limit issue of alkenone-based SST estimation. The sites located in the western Pacific warm pool are ODP 806 and ODP 1143, and the sites located in the eastern tropical Pacific include ODP 846 (3.09°S, 90.82°W), ODP 847, ODP 850, ODP 1237, ODP 1239 (0.67°S, 82.08°W), ODP 1241 (5.84°N, 86.44°W), and Integrated Ocean Drilling Project (IODP) site U1338 (2.51°N, 117.97°W). We used median values at each site for estimating SST anomalies during the mid-Pliocene relative to pre-industrial shown in Fig. 3a and ensemble-mean values averaged over the western Pacific warm pool and the eastern equatorial Pacific for the time series of zonal SST difference shown in Supplementary Fig. 7c. In addition, a reconstructed Pliocene Pacific SST field derived from alkenone proxy data⁴⁴ is used in this study.

For the case of LGM SSTs, we used geochemical proxy records from ref. 49. Given conflicting proxy reconstructions for the LGM period^{19,64,65}, we also used paleoclimate data assimilation products^{49,51,52}, in which large uncertainties stemming from incomplete and uneven proxy data sampling in both space and time were substantially reduced. In particular, ref. 49 exclusively used geochemical SST proxies (i.e., the unsaturation index of alkenones, TEX₈₆, $\delta^{18}\text{O}$ and the Mg/Ca ratio) to avoid no-analog problems and lack of comparable Bayesian models.

Ref. 43 produced a global SST stack covering the last 4.5 million years using 127 published SST records based on alkenone, Mg/Ca ratio, and faunal proxies with taking into account long-term changes in seawater Mg/Ca ratio and used the global SST stack to reconstruct global-mean surface temperature change over the same period by applying a scaling formula derived from climate model simulations. These paleoclimate temperature data are used to estimate the temporal evolution of global-mean surface temperature as well as the zonal SST difference between sites located in the western Pacific warm pool and sites located in the eastern tropical Pacific (Fig. 4 and Supplementary Fig. 7). It is noted that the temporal evolution of global-mean surface temperature estimated from ref. 43 is qualitatively consistent with that from ref. 66 and ref. 67 (Supplementary Fig. 7a).

Model simulation output

The temporal evolution of model-simulated tropical Pacific zonal SST and SLP gradients is evaluated over the period 1950–2100 using the Community Earth System Model version 2 Large Ensemble (CESM2 LE) simulations⁵ forced with CMIP6⁶⁸ historical forcing over the period 1850–2014 and Shared Socioeconomic Pathway (SSP) forcing scenario SSP3-7.0 over the period 2015–2100. The CESM2 LE consists of two 50-member subsets, but we only used the second subset forced by a smoothed version of the biomass burning dataset over the period 1990–2020. Detailed information on the CESM2 LE initialization procedure can be found in ref. 5. Given large inter-model spread, CanESM5 is also used to examine whether the time duration of the instrumental record is sufficiently long for confidently determining the forced response. We used simulation output for 50 ensemble members forced by the CMIP6 historical protocol and the SSP3-7.0 scenario.

The GFDL-ESM2M model is exceptional in that a La Niña-like mean state change is simulated in response to greenhouse gas forcing²⁷ standing in contrast to other models that produce an El Niño-like mean state change. However, given that simulation output from a single ensemble member was analyzed in ref. 27, it is uncertain whether the reported La Niña-like mean state change is a forced response due to the potential role of internal variability^{30,33,34,69,70}. For this reason, along with the CESM2 LE and CanESM5, we analyzed the GFDL-ESM2M Large Ensemble⁷¹, which consists of 30 ensemble members run under CMIP5 historical forcing

(1850–2004) and subsequently the Representative Concentration Pathway (RCP) 8.5 scenario.

Working under the assumption that a qualitative agreement with paleoclimate proxy record lends some credence to the robustness of model-projected future climate change under sustained anthropogenic forcing, model simulation output for the CMIP6-PMIP4 midPliocene-eoi400 was evaluated against the paleoclimate proxy data described in the preceding subsection. The midPliocene-eoi400 experiment was designed to examine the response of the climate system to stable long-term CO₂ forcing (~400 ppm), similar to the present day, during the mid-Pliocene warm period (~3.2 million years ago) when mean surface temperature was warmer than that for the pre-industrial period^{43,44,46}. In the midPliocene-eoi400 experiment, astronomical parameters, solar activity, and tropospheric aerosols were prescribed as in the pre-industrial control experiment, while the experimental design included modifications to ice sheets, topography, ocean bathymetry, and vegetation. On the premise that there is a causal relationship between CO₂ forcing (or global warming) and changes in the zonal SST gradient, we also analyzed the CMIP6-PMIP4 lgm experiment which focuses on the LGM period (~21 thousand years ago) when CO₂ concentrations were ~200 ppm with boundary conditions being substantially different from the present day. We note that the magnitude of the changes in forcing and global mean surface temperature between the LGM and pre-industrial periods is comparable to that projected from the present to the end of the 21st century⁷². More detailed information on the CMIP6-PMIP4 midPliocene-eoi400 and lgm experiments can be found in ref. 73 and in ref. 72, respectively.

Although the CESM2 LE simulations do not encompass these periods in the relatively distant past, CESM2 was a contributing model to the midPliocene-eoi400 group of simulations under CMIP6-PMIP4. Additionally, CESM2-FV2 and CESM2-WACCM-FV2, which are closely related to CESM2⁷⁴, were also contributions to the CMIP6-PMIP4 lgm exercise. Hence, these model simulations along with corresponding pre-industrial control simulations are used in our analysis. Considering that there are potentially large model structural uncertainties across CMIP6 models, we also included additional CMIP6 models participating in the CMIP6-PMIP4: EC-Earth3-LR, GISS-E2-1-G, HadGEM3-GC31-LL, IPSL-CM6A-LR, and NorESM1-F for the midPliocene-eoi400 experiment and INM-CM4-8, MIROC-ES2L, and MPI-ESM1-2-LR for the lgm experiment.

To examine whether climate models are able to reproduce the relationship inferred from paleoclimate proxy records between global-mean surface temperature and the zonal SST gradient, we analyzed a range of idealized experiments along with the midPliocene-eoi400 and lgm, i.e., abrupt-4×CO₂ (coupled model simulation in which atmospheric CO₂ concentrations were abruptly quadrupled from pre-industrial levels and then were held fixed for at least 150 years), abrupt-0.5×CO₂ (similar to abrupt-4×CO₂, except that CO₂ concentrations were abruptly halved), abrupt-solp4p (similar to abrupt-4×CO₂, except that the solar constant was instantaneously increased by 4%), and abrupt-solm4p (similar to abrupt-solp4p, except that the solar constant was reduced by 4%). For these idealized experiments forced by abrupt change, we analyzed SST and SLP anomalies averaged over years 131–150 relative to pre-industrial values. Supplementary Table 1 provides information on the model simulations analyzed in this study.

Statistical information

We used the standard least squares linear regression approach for computing trends. Statistical significance of the computed trends is determined using a two-sided Student's *t*-test at the 95% confidence level with reduced degrees of freedom to account for autocorrelation in a given time series.

Data availability

The ERSST5 data set is available at <https://psl.noaa.gov/data/gridded/data.noaa.ersst.v5.html>, the HadISST data set at <https://www.metoffice.gov.uk/hadobs/hadisst/data/download.html>, the ERA5 data set at <https://cds.climate.copernicus.eu>, the JRA-55 data set at <https://rda.ucar.edu/datasets/>

ds628.0/, the COBE-SST2 dataset at <https://psl.noaa.gov/data/gridded/data.cobe2.html>, the PRISM3 dataset at https://geology.er.usgs.gov/egpsc/prism/prism_1_23/prism_data.html, the TEX₈₆ and alkenone temperature proxy data at <https://www.science.org/doi/10.1126/science.1246172>, the alkenone-based temperature proxy data at <https://agupubs.onlinelibrary.wiley.com/doi/abs/10.1029/2019GL083802>, LGM geochemical proxy records at <https://github.com/jesstierney/lgmDA/tree/master/version2.1>, paleoclimate data assimilation products at <https://github.com/jesstierney/lgmDA/tree/master/version2.1>, <https://www.ncei.noaa.gov/access/paleo-search/study/33112> and <https://doi.org/10.5194/cp-18-1883-2022>, the global-mean surface temperature and zonal SST gradient anomalies over the past four million years at <https://doi.org/10.1126/science.ad1908>, CO₂ concentrations at <https://paleo-co2.org>, the CESM2 Large Ensemble output at <https://www.cesm.ucar.edu/projects/community-projects/LENS2/datasets.html>, the CMIP5 and CMIP6 simulation output at <https://aims2.llnl.gov/search>, and the GFDL-ESM2M Large Ensemble output at <https://www.cesm.ucar.edu/community-projects/mmllea>. The data for replicating the main figures in this study are available at <https://doi.org/10.5281/zenodo.14575519>.

Code availability

Most figures are generated using the NCAR Command Language (NCL, Version 6.6.2, <https://doi.org/10.5065/D6WD3XH5>). The codes used to generate the main figures in this study are freely available at <https://doi.org/10.5281/zenodo.14575519>.

Received: 10 October 2024; Accepted: 15 January 2025;

Published online: 08 February 2025

References

1. Collins, M. et al. The impact of global warming on the tropical Pacific Ocean and El Niño. *Nat. Geosci.* **3**, 391–397 (2010).
2. Cai, W. et al. Changing El Niño-Southern oscillation in a warming climate. *Nat. Rev. Earth Environ.* **2**, 628–644 (2021).
3. Meehl, G. A., Arblaster, J. M., Bitz, C. M., Chung, C. T. Y. & Teng, H. Antarctic sea-ice expansion between 2000 and 2014 driven by tropical Pacific decadal climate variability. *Nat. Geosci.* **9**, 590–595 (2016).
4. Li, X. et al. Tropical teleconnection impacts on Antarctic climate changes. *Nat. Rev. Earth Environ.* **2**, 680–698 (2021).
5. Rodgers, K. B. et al. Ubiquity of human-induced changes in climate variability. *Earth. Syst. Dynam.* **12**, 1393–1411 (2021).
6. Chung, E.-S. et al. Antarctic sea-ice expansion and Southern Ocean cooling linked to tropical variability. *Nat. Clim. Change* **12**, 461–468 (2022).
7. Li, X., Hu, Z.-Z., McPhaden, M. J., Zhu, C. & Liu, Y. Triple-dip La Niñas in 1998–2001 and 2020–2023: Impact of mean state changes. *J. Geophys. Res. Atmos.* **128**, e2023JD038843 (2023).
8. Cane, M. A. et al. Twentieth-century sea surface temperature trends. *Science* **275**, 957–960 (1997).
9. Dong, Y., Proistosescu, C., Armour, K. C. & Battisti, D. S. Attributing historical and future evolution of radiative feedbacks to regional warming patterns using a Green's function approach: The preeminence of the Western Pacific. *J. Clim.* **32**, 5471–5491 (2019).
10. Dong, Y., Pauling, A. G., Sadai, S. & Armour, K. C. Antarctic ice-sheet meltwater reduces transient warming and climate sensitivity through the sea-surface temperature pattern effect. *Geophys. Res. Lett.* **49**, e2022GL101249 (2022).
11. Kang, S. M. et al. Global impacts of recent Southern Ocean cooling. *Proc. Natl. Acad. Sci. USA* **120**, e2300881120 (2023).
12. Latif, M. et al. Strengthening atmospheric circulation and trade winds slowed tropical Pacific surface warming. *Commun. Earth Environ.* **4**, 249 (2023).
13. Lee, S. et al. On the future zonal contrasts of equatorial Pacific climate: Perspectives from observations, simulations, and theories. *npj Clim. Atmos. Sci.* **5**, 82 (2022).

14. Hartmann, D. L. The Antarctic ozone hole and the pattern effect on climate sensitivity. *Proc. Natl Acad. Sci. USA* **119**, e2207889119 (2022).
15. Watanabe, M. et al. Possible shift in controls of the tropical Pacific surface warming pattern. *Nature* **630**, 315–324 (2024).
16. DiNezio, P. N. et al. Climate response of the equatorial Pacific to global warming. *J. Clim.* **22**, 4873–4892 (2009).
17. Seager, R. et al. Strengthening tropical Pacific zonal sea surface temperature gradient consistent with rising greenhouse gases. *Nat. Clim. Change* **9**, 517–522 (2019).
18. Seager, R., Henderson, N. & Cane, M. Persistent discrepancies between observed and modeled trends in the tropical Pacific Ocean. *J. Clim.* **35**, 4571–4584 (2022).
19. Heede, U. K. & Fedorov, A. V. Eastern equatorial Pacific warming delayed by aerosols and thermostat response to CO₂ increase. *Nat. Clim. Change* **11**, 696–703 (2021).
20. Wills, R. C. J., Dong, Y., Proistosecu, C., Armour, K. C. & Battisti, D. S. Systematic climate model biases in the large-scale patterns of recent sea-surface temperature and sea-level pressure change. *Geophys. Res. Lett.* **49**, e2022GL100011 (2022).
21. Knutson, T. R. & Manabe, S. Time-mean response over the tropical Pacific to increased CO₂ in a coupled ocean-atmosphere model. *J. Clim.* **8**, 2181–2199 (1995).
22. Held, I. M. & Soden, B. J. Robust responses of the hydrological cycle to global warming. *J. Clim.* **19**, 5686–5699 (2006).
23. McGregor, S. et al. Recent Walker circulation strengthening and Pacific cooling amplified by Atlantic warming. *Nat. Clim. Change* **4**, 888–892 (2014).
24. Chung, E.-S. et al. Reconciling opposing Walker circulation trends in observations and model projections. *Nat. Clim. Change* **9**, 405–412 (2019).
25. Yun, K.-S., Timmermann, A. & Stuecker, M. F. Synchronized spatial shifts of Hadley and Walker circulations. *Earth Syst. Dynam.* **12**, 121–132 (2021).
26. Clement, A. C., Seager, R., Cane, M. A. & Zebiak, S. E. An ocean dynamical thermostat. *J. Clim.* **9**, 2190–2196 (1996).
27. Kohyama, T., Hartmann, D. L. & Battisti, D. S. La Niña-like mean-state response to global warming and potential oceanic roles. *J. Clim.* **30**, 4207–4225 (2017).
28. Kim, H., Kang, S. M., Kay, J. E. & Xie, S.-P. Subtropical clouds key to Southern Ocean teleconnections to the tropical Pacific. *Proc. Natl Acad. Sci. USA* **119**, e2200514119 (2022).
29. Heede, U. K. & Fedorov, A. V. Colder eastern equatorial Pacific and stronger Walker circulation in the early 21st century: Separating the forced response to global warming from natural variability. *Geophys. Res. Lett.* **50**, e2022GL101020 (2023).
30. Chung, E.-S. et al. Tropical eastern Pacific cooling trend reinforced by human activity. *npj Clim. Atmos. Sci.* **7**, 170 (2024).
31. Takahashi, C. & Watanabe, M. Pacific trade winds accelerated by aerosol forcing over the past two decades. *Nat. Clim. Change* **6**, 768–772 (2016).
32. Hwang, Y.-T., Xie, S.-P., Chen, P.-J., Tseng, H.-Y. & Deser, C. Contribution of anthropogenic aerosols to persist La Niña-like conditions in the early 21st century. *Proc. Natl Acad. Sci. USA* **121**, e2315124121 (2024).
33. Olonscheck, D., Rugenstein, M. & Marotzke, J. Broad consistency between observed and simulated trends in sea surface temperature patterns. *Geophys. Res. Lett.* **47**, e2019GL086773 (2020).
34. Watanabe, M., Dufresne, J.-L., Kosaka, Y., Mauritsen, T. & Tatebe, H. Enhanced warming constrained by past trends in equatorial Pacific sea surface temperature gradient. *Nat. Clim. Change* **11**, 33–37 (2021).
35. Vecchi, G. A., Clement, A. & Soden, B. J. Examining the tropical Pacific's response to global warming. *Eos Trans. AGU* **89**, 81–83 (2008).
36. Karnauskas, K. B., Seager, R., Kaplan, A., Kushnir, Y. & Cane, M. A. Observed strengthening of the zonal sea surface temperature gradient across the equatorial Pacific Ocean. *J. Clim.* **22**, 4316–4321 (2009).
37. Deser, C., Phillips, A. S. & Alexander, M. A. Twentieth century tropical sea surface temperature trends revisited. *Geophys. Res. Lett.* **37**, L10701 (2010).
38. Han, T. et al. Corals evidence an underestimation of the 20th century warming in the eastern Pacific cold tongue. *Geophys. Res. Lett.* **51**, e2024GL108954 (2024).
39. Vecchi, G. A. et al. Weakening of tropical Pacific atmospheric circulation due to anthropogenic forcing. *Nature* **441**, 73–76 (2006).
40. Tokinaga, H., Xie, S.-P., Deser, C., Kosaka, Y. & Okumura, Y. M. Slowdown of the Walker circulation driven by tropical Indo-Pacific warming. *Nature* **491**, 439–443 (2012).
41. Kageyama, M. et al. The PMIP4 contribution to CMIP6 – Part 1: Overview and over-arching analysis plan. *Geosci. Model Dev.* **11**, 1033–1057 (2018).
42. Tierney, J. E. et al. Past climates inform our future. *Science* **370**, eaay3701 (2020).
43. Clark, P. U., Shakun, J. D., Rosenthal, Y., Köhler, P. & Bartlein, P. J. Global and regional temperature change over the past 4.5 million years. *Science* **383**, 884–890 (2024).
44. Tierney, J. E., Haywood, A. M., Feng, R., Bhattacharya, T. & Otto-Bliesner, B. L. Pliocene warmth consistent with greenhouse gas forcing. *Geophys. Res. Lett.* **46**, 9136–9144 (2019).
45. Ravelo, A. C., Lawrence, K. T., Fedorov, A. & Ford, H. L. Comment on “A 12-million-year temperature history of the tropical Pacific”. *Science* **346**, 1467–1467 (2014).
46. Dowsett, H. J. et al. Assessing confidence in Pliocene sea surface temperatures to evaluate predictive models. *Nat. Clim. Change* **2**, 365–371 (2012).
47. Zhang, Y. G., Pagani, M. & Liu, Z. A 12-million-year temperature history of the tropical Pacific Ocean. *Science* **344**, 84–87 (2014).
48. Lea, D. W. Not so permanent El Niño. *Science* **344**, 52–53 (2014).
49. Tierney, J. E. et al. Glacial cooling and climate sensitivity revisited. *Nature* **584**, 569–573 (2020).
50. Thirumalai, K. et al. Future increase in extreme El Niño supported by past glacial changes. *Nature* **634**, 374–380 (2024).
51. Osman, M. B. et al. Globally resolved surface temperatures since the Last Glacial Maximum. *Nature* **599**, 239–244 (2021).
52. Annan, J. D., Hargreaves, J. C. & Mauritsen, T. A new global surface temperature reconstruction for the Last Glacial Maximum. *Clim. Past* **18**, 1883–1896 (2022).
53. Yan, Q. et al. Large shift of the Pacific Walker circulation across the Cenozoic. *Natl Sci. Rev.* **8**, nwaa101 (2021).
54. Huang, B. et al. Extended Reconstructed Sea Surface Temperature, Version 5 (ERSSTv5): Upgrades, validations, and intercomparisons. *J. Clim.* **30**, 8179–8205 (2017).
55. Rayner, N. A. et al. Global analyses of sea surface temperature, sea ice, and night marine air temperature since the late nineteenth century. *J. Geophys. Res.* **108**, 4407 (2003).
56. Hersbach, H. et al. The ERA5 global reanalysis. *Q. J. R. Meteorol. Soc.* **146**, 1999–2049 (2020).
57. Kobayashi, S. et al. The JRA-55 Reanalysis: General specifications and basic characteristics. *J. Meteor. Soc. Japan* **93**, 5–48 (2015).
58. Hirahara, S., Ishii, M. & Fukuda, Y. Centennial-scale sea surface temperature analysis and its uncertainty. *J. Clim.* **27**, 57–75 (2014).
59. Dowsett, H. J., Robinson, M. M. & Foley, K. M. Pliocene three-dimensional global ocean temperature reconstruction. *Clim. Past* **5**, 769–783 (2009).
60. Dowsett, H. J. et al. The PRISM3D paleoenvironmental reconstruction. *Stratigraphy* **7**, 123–139 (2010).

61. Levitus, S. & Boyer, T. P. *World Ocean Atlas* 1994. Vol. 4, Temperature. NOAA Atlas NESDIS 4, U.S. Department of Commerce, NOAA, Washington, D.C. (1994).

62. Reynolds, R. W. & Smith, T. M. A high-resolution global sea surface temperature climatology. *J. Clim.* **8**, 1571–1583 (1995).

63. Kim, J. H. et al. New indices and calibrations derived from the distribution of crenarchaeal isoprenoid tetraether lipids: Implications for past sea surface temperature reconstructions. *Geochim. Cosmochim. Acta* **74**, 4639–4654 (2010).

64. Ford, H. L., Ravelo, A. C. & Polissar, P. J. Reduced El Niño–Southern oscillation during the Last Glacial Maximum. *Science* **347**, 255–258 (2015).

65. Monteagudo, M. M., Lynch-Stieglitz, J., Marchitto, T. M. & Schmidt, M. W. Central equatorial Pacific cooling during the Last Glacial Maximum. *Geophys. Res. Lett.* **48**, e2020GL088592 (2021).

66. Hansen, J., Sato, M., Russell, G. & Kharecha, P. Climate sensitivity, sea level and atmospheric carbon dioxide. *Philos. Trans. A Math. Phys. Eng. Sci.* **371**, 20120294 (2013).

67. Snyder, C. W. Evolution of global temperature over the past two million years. *Nature* **538**, 226–228 (2016).

68. Eyring, V. et al. Overview of the Coupled Model Intercomparison Project Phase 6 (CMIP6) experimental design and organization. *Geosci. Model Dev.* **9**, 1937–1958 (2016).

69. Dong, L. & Zhou, T. The formation of the recent cooling in the eastern tropical Pacific Ocean and the associated climate impacts: A competition of global warming, IPO, and AMO. *J. Geophys. Res. Atmos.* **119**, 11,272–11,287 (2014).

70. Meehl, G. A., Hu, A., Arblaster, J. M., Fasullo, J. & Trenberth, K. E. Externally forced and internally generated decadal climate variability associated with the Interdecadal Pacific Oscillation. *J. Clim.* **26**, 7298–7310 (2013).

71. Rodgers, K. B., Lin, J. & Frölicher, T. L. Emergence of multiple ocean ecosystem drivers in a large ensemble suite with an Earth system model. *Biogeosciences* **12**, 3301–3320 (2015).

72. Kageyama, M. et al. The PMIP4 contribution to CMIP6 – Part 4: Scientific objectives and experimental design of the PMIP4-CMIP6 Last Glacial Maximum experiments and PMIP4 sensitivity experiments. *Geosci. Model Dev.* **10**, 4035–4055 (2017).

73. Haywood, A. M. et al. The Pliocene Model Intercomparison Project (PlioMIP) Phase 2: scientific objectives and experimental design. *Clim. Past* **12**, 663–675 (2016).

74. Zhang, Q., Liu, B., Li, S. & Zhou, T. Understanding model's global sea surface temperature bias in mean state: From CMIP5 to CMIP6. *Geophys. Res. Lett.* **50**, e2022GL100888 (2023).

Acknowledgements

We thank anonymous reviewers and the editor for their constructive and valuable comments, which led to an improved version of the manuscript. We are grateful to the National Oceanic and Atmospheric Administration Physical Sciences Laboratory, the Met Office Hadley Centre, the European Centre for Medium Range Weather Forecasts, National Center for Atmospheric Research, modeling centers contributing to the CMIP5 and CMIP6, PRISM3D Project, Jessica Tierney, Yi Ge Zhang, and Peter Clark for providing their respective data sets. E.-S.C., S.-J.K., S.-Y.J. and J.-H.K. were supported by Korea Polar Research Institute (KOPRI) grant funded by

the Ministry of Oceans and Fisheries (KOPRI PE25030). E.-S.C. was also supported by KOPRI grant PE23340. K.B.R., S.-S.L. and K.-S.Y. were supported by the Institute for Basic Science (IBS) under IBS-R028-D1. K.B.R. was also supported by the World Premier International Research Center Initiative, MEXT, Japan.

Author contributions

E.-S.C. and S.-J.K. designed the study. E.-S.C. performed the analysis and produced figures. S.-J.K., K.B.R., S.-Y.J., J.-H.K., S.-S.L. and K.-S.Y. provided feedback on the analysis, interpretation of the results, and the figures. All authors contributed to the writing of the manuscript and the improvement of the manuscript.

Competing interests

The authors declare no competing interests. K.-S.Y. is an Editorial Board Member for Communications Earth & Environment, but was not involved in the editorial review of, nor the decision to publish this article.

Additional information

Supplementary information The online version contains supplementary material available at <https://doi.org/10.1038/s43247-025-02039-0>.

Correspondence and requests for materials should be addressed to Seong-Joong Kim.

Peer review information *Communications Earth & Environment* thanks the anonymous reviewers for their contribution to the peer review of this work. Primary Handling Editor: Alireza Bahadori. A peer review file is available.

Reprints and permissions information is available at <http://www.nature.com/reprints>

Publisher's note Springer Nature remains neutral with regard to jurisdictional claims in published maps and institutional affiliations.

Open Access This article is licensed under a Creative Commons Attribution-NonCommercial-NoDerivatives 4.0 International License, which permits any non-commercial use, sharing, distribution and reproduction in any medium or format, as long as you give appropriate credit to the original author(s) and the source, provide a link to the Creative Commons licence, and indicate if you modified the licensed material. You do not have permission under this licence to share adapted material derived from this article or parts of it. The images or other third party material in this article are included in the article's Creative Commons licence, unless indicated otherwise in a credit line to the material. If material is not included in the article's Creative Commons licence and your intended use is not permitted by statutory regulation or exceeds the permitted use, you will need to obtain permission directly from the copyright holder. To view a copy of this licence, visit <http://creativecommons.org/licenses/by-nc-nd/4.0/>.

© The Author(s) 2025